Electronic Supplementary Material (ESI) for RSC Advances.

Supporting Information

Highly specific probe for dual-emissive mitochondrial imaging based on photostable and aqueous-soluble phosphonium fluorophore

Gaocan Li, Ke Yang, Jing Sun,* and Yunbing Wang*

National Engineering Research Center for Biomaterials, Sichuan University, 29 Wangjiang Road, Chengdu 610064, China

E-mail: jingsun@scu.edu.cn; yunbing.wang@scu.edu.cn

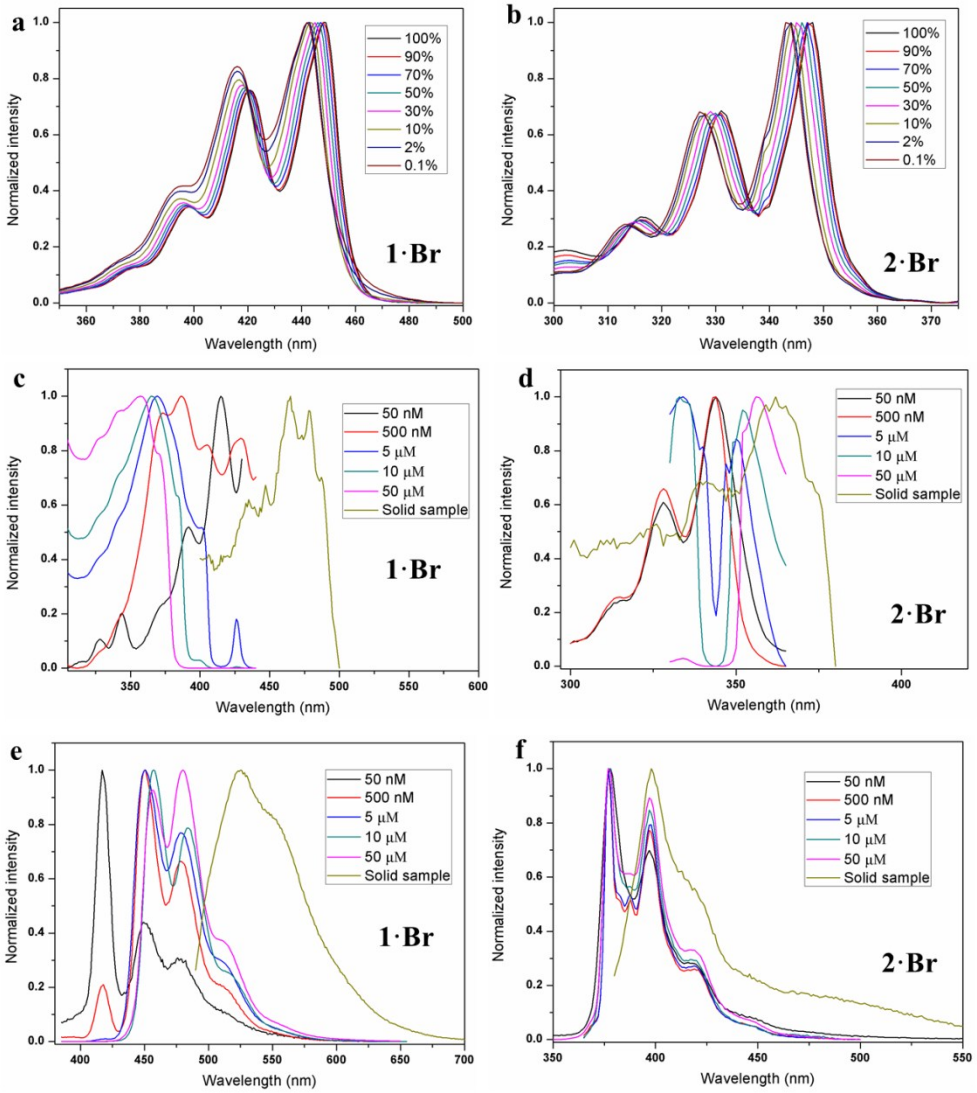

Figure S1. Absorption spectra recorded in DMSO/H_2O with different fraction of DMSO (v/v): a) 30 μm; b) 40 μm. Normalized excitation and emission spectra of the aqueous solution with increasing concentrations and solid samples of **1·Br** and **2·Br**: c) and d) excitation spectra; e) and f) emission spectra, excited at the corresponding maximum excitation wavelength.

The absorption of **1·Br** and **2·Br** recorded in DMSO/H_2O with different fraction of DMSO indicated that blue-shifts of the absorption of **1·Br** and **2·Br** could be observed with the increasing fraction of water, which suggested that the H-type aggregation could be formed for **1·Br** and **2·Br** with the decreasing fraction of DMSO (Figure S1a and S1b). There is a large emission range from 417 nm to 525 nm can be observed for **1·Br** in different states (Figure S1e). However, all the emissions of **2·Br** from the solution to the solid state are located in the range of blue light with

the emission wavelength from 378 nm to 398 nm (Figure S1f), which results in the cell imaging with single blue luminescence for **2·Br**.

Table S1. Photophysical properties of phosphonium salt **1·Br** in different concentrations.

Concentration	$(\Phi_f)^a$	τ (ns) (χ^2)
500 nM	0.12	4.96 (1.04)
5 μM	0.17	5.04 (1.05)
10 μM	0.65	5.10 (1.11)
50 μM	0.89	5.40 (1.04)
solid	0.14	2.45 (1.16)

[a]Absolute emission quantum yields estimated by calibrated integrating sphere system. Φ_f: quantum yield. τ: lifetime.

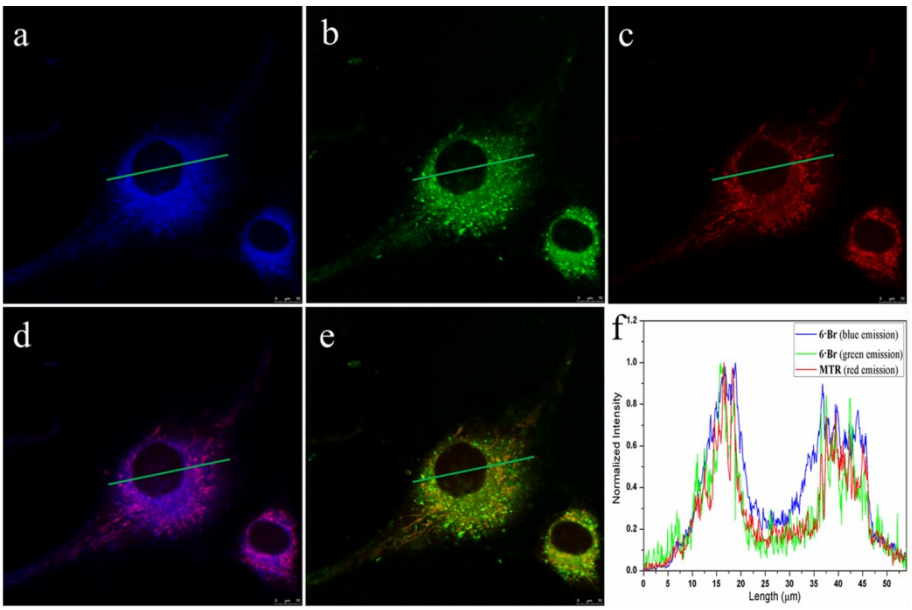

Figure S2. Co-staining of MG63 cells with phosphonium salt **1·Br** (3.0 μM) and **MTR** (500.0 nM): a) blue fluorescent image of MG63 cells stained with **1·Br** for 1 h (λ_{ex} = 408 nm, λ_{em} = 420−470 nm); b) green fluorescent image of MG63 cells stained with **1·Br** for 1 h (λ_{ex} = 488 nm, λ_{em} = 510−560 nm); c) red fluorescent image of MG63 cells stained with **MTR** for 0.5 h (λ_{ex} = 552 nm, λ_{em} = 620−680 nm); d) merged images of a) and c); e) merged images of b) and c); and f) intensity profile of regions across MG63 cell.

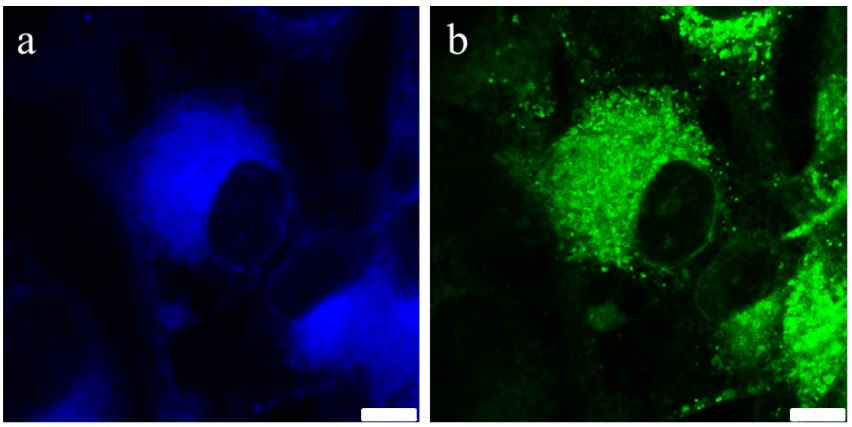

Figure S3. Confocal fluorescence images of CCCP (10 μM) treated MG63 cells cultured with **1·Br** (5.0 μM) for 1 h: a) under irradiation at 405 nm (λ_{em} = 420−470 nm); b) under irradiation at 488 nm (λ_{em} = 510−560 nm). Scale bar: 7.5 μm.

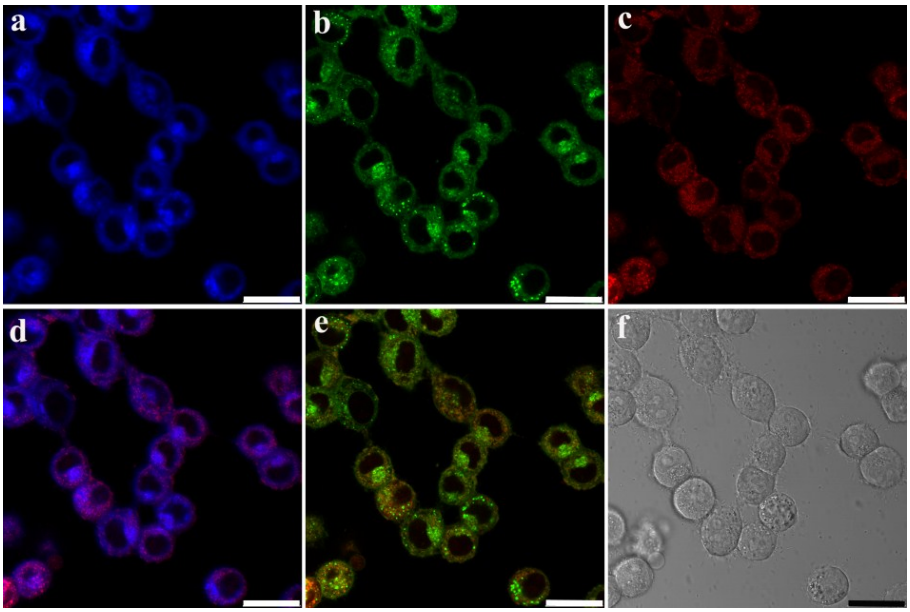

Figure S4. Co-staining of MG63 cells with phosphonium salt **1·PF$_6$** (3.0 μM) and **MTR** (500.0 nM): a) blue fluorescent image of MG63 cells stained with **1·PF$_6$** for 1 h (λ_{ex} = 408 nm, λ_{em} = 420−470 nm); b) green fluorescent image of MG63 cells stained with **1·PF$_6$** for 1 h (λ_{ex} = 488 nm, λ_{em} = 510−560 nm); c) red fluorescent image of MG63 cells stained with **MTR** for 0.5 h (λ_{ex} = 552 nm, λ_{em} = 620−680 nm); d) merged images of a) and c); e) merged images of b) and c); and f) bright-field image. Scale bar: 25 μm.

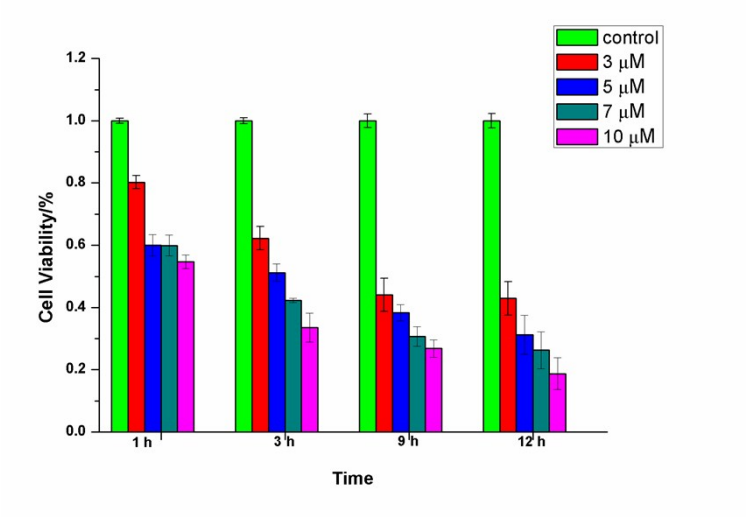

Figure S5. Cell viability of MG63 cells incubated with increasing concentrations of **1·PF$_6$** at 37 ºC for different amounts of time.

The co-staining experiments of MG63 cells with **1·PF$_6$** (phosphonium salt **1** with PF_6^- as the counteranion) and red-fluorescent tracker MitoTracker Red FM (**MTR**) has also been investigated (Figure S4). The Pearson's coefficient (*R*r = 0.71) and Manders' coefficients (m_1 = 0.93 and m_2 = 0.99) for the blue and red fluorescence images and the Pearson's coefficient (*R*r = 0.75) and Manders' coefficients (m_1 = 0.97 and m_2 = 0.98) for the green and red fluorescence images clearly demonstrated the specific targeting to the mitochondria of living cells. The phosphonium salt **1·PF$_6$** exhibited poor solubility in water and relatively higher cytotoxicity (Figure S5), which might caused the slight decrease of specificity to the mitochondria compared to **1·Br**.

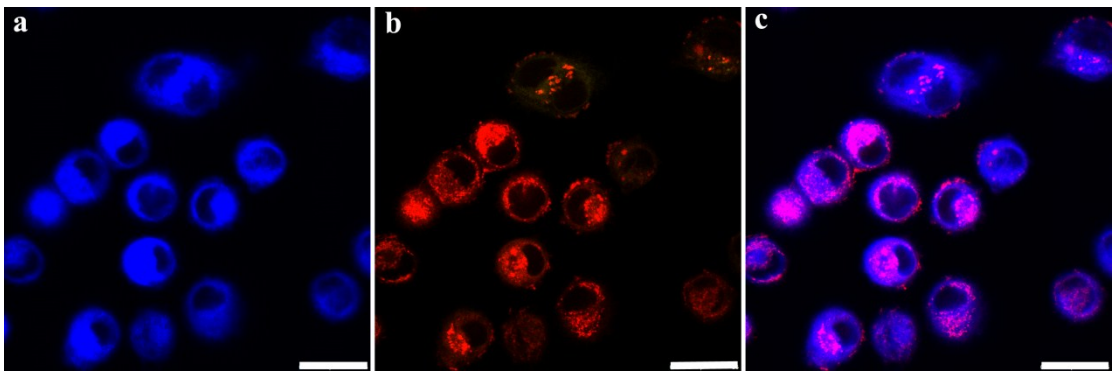

Figure S6. Co-staining of MG63 cells with phosphonium salt **2·Br** (3.0 μM) and **MTR** (500.0 nM): a) blue fluorescent image of MG63 cells stained with **2·Br** for 1 h (λ_{ex} = 408 nm, λ_{em} = 420−470 nm); b) red fluorescent image of MG63 cells stained with **MTR** for 0.5 h (λ_{ex} = 552 nm, λ_{em} = 620−680 nm); and c) merged images of a) and b). Scale bar: 25 μm.

The co-staining experiments of MG63 cells with **2·Br** and red-fluorescent tracker MitoTracker Red FM (**MTR**) were also conducted. The Pearson's coefficient (*R*r = 0.64) and Manders' coefficients (m_1 = 0.89 and m_2 = 0.99) for the blue and red fluorescence images were obtained, which demonstrated a lower specificity to the mitochondria compared to **1·Br**. It was suggesting that the lipophilicity might be another factor facilitating the entrance of probes into mitochondria and the relatively strong lipophilicity of **1·Br** might also have significant effect on the specificity to mitochondria beside the electrophoretic force.

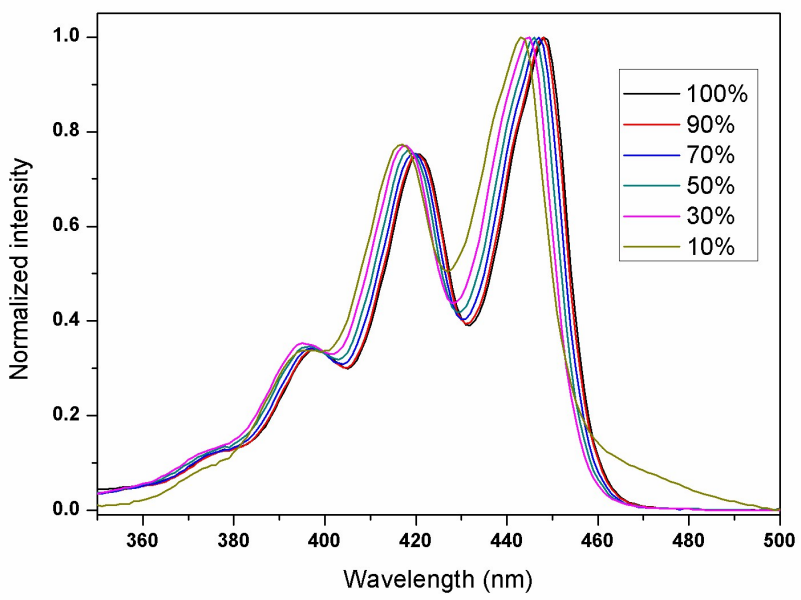

Figure S7. Absorption spectra of **1·PF$_6$** (10 μm) recorded in DMSO/H_2O with different fraction of DMSO (v/v).

The phosphonium salt **1·PF$_6$** exhibited poor solubility in water. As shown in Figure S7, a blue-shift of the absorption of **1·PF$_6$** could be observed with the increasing fraction of water, which suggested that the H-type aggregation could be formed for **1·PF$_6$** with the decreasing fraction of DMSO.

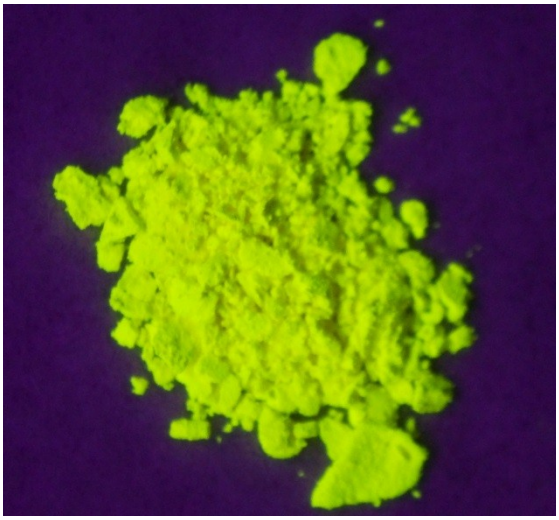

Figure S8. Photographs of the solid of **1**·**Br** under UV irradiation at 365 nm.

Copies of ^{1}H, ^{13}C and ^{31}P NMR spectra

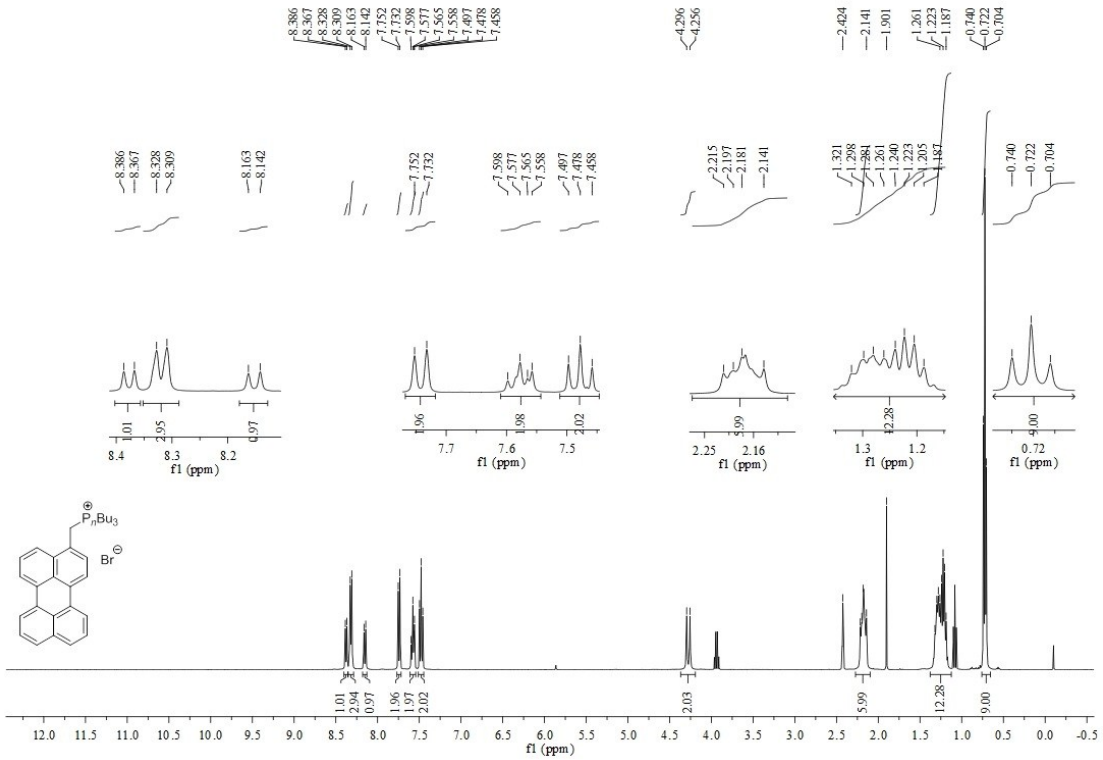

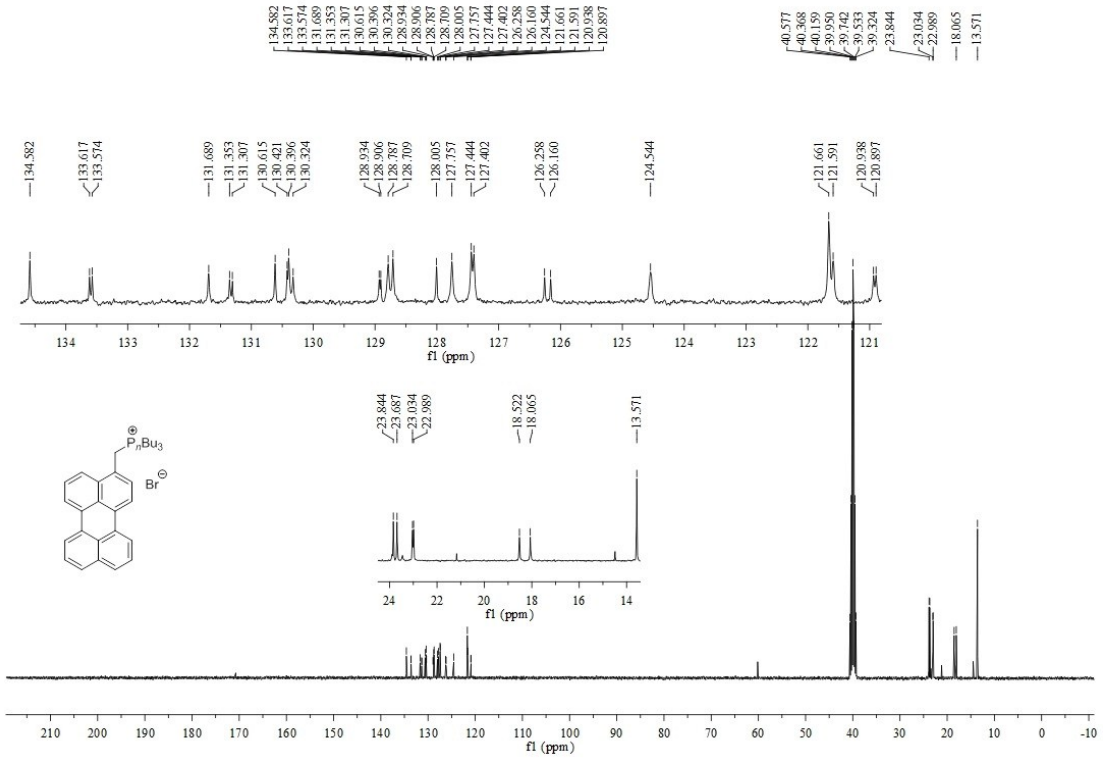

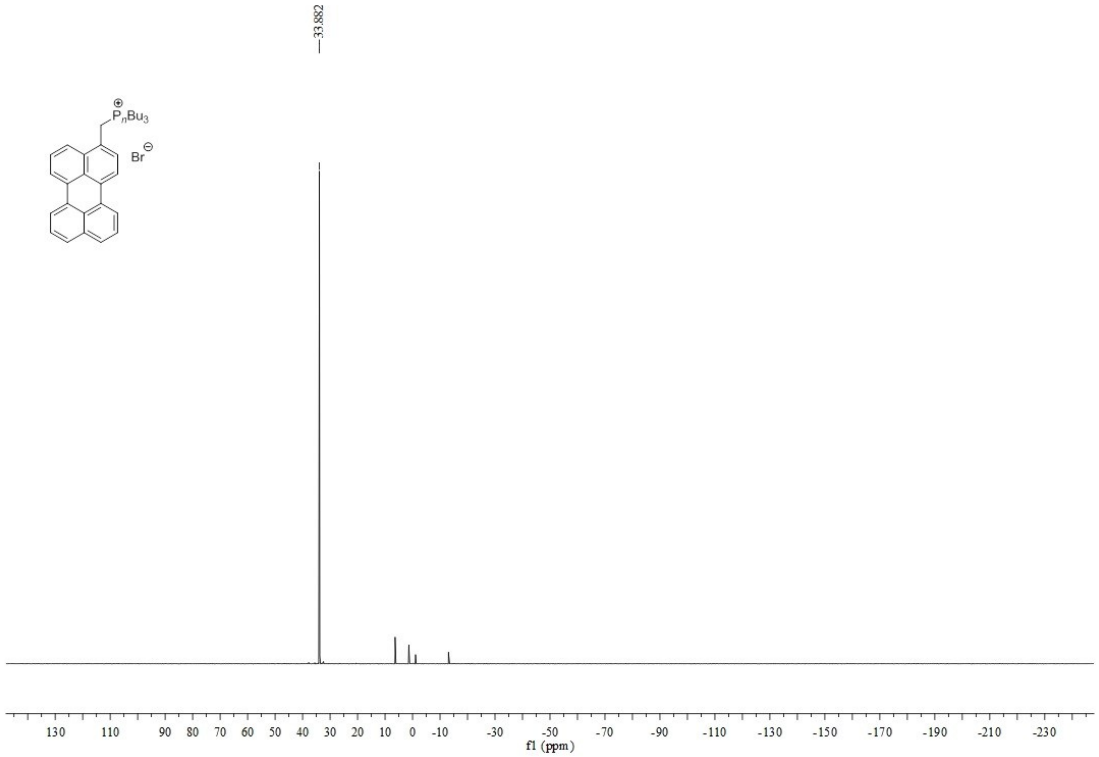
33.882
P$_n$Bu$_3$
Br
f1 (ppm)

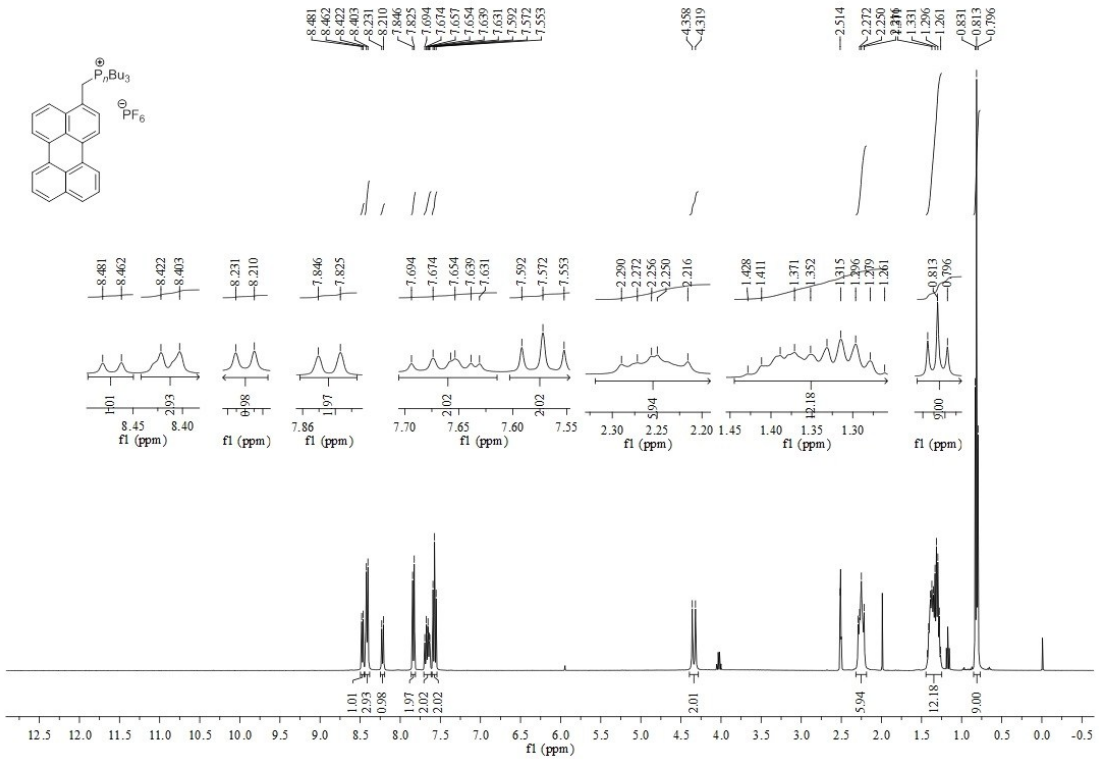
8.481
8.462
8.422
8.403
8.231
8.210
7.846
7.825
7.694
7.674
7.654
7.639
7.631
7.592
7.572
7.553
4.358
4.319
2.514
2.272
2.250
1.331
1.296
1.261
0.831
0.813
0.796
P$_n$Bu$_3$
PF$_6$
1.01
2.93
0.98
1.97
2.02
2.02
2.01
5.94
12.18
9.00
f1 (ppm)

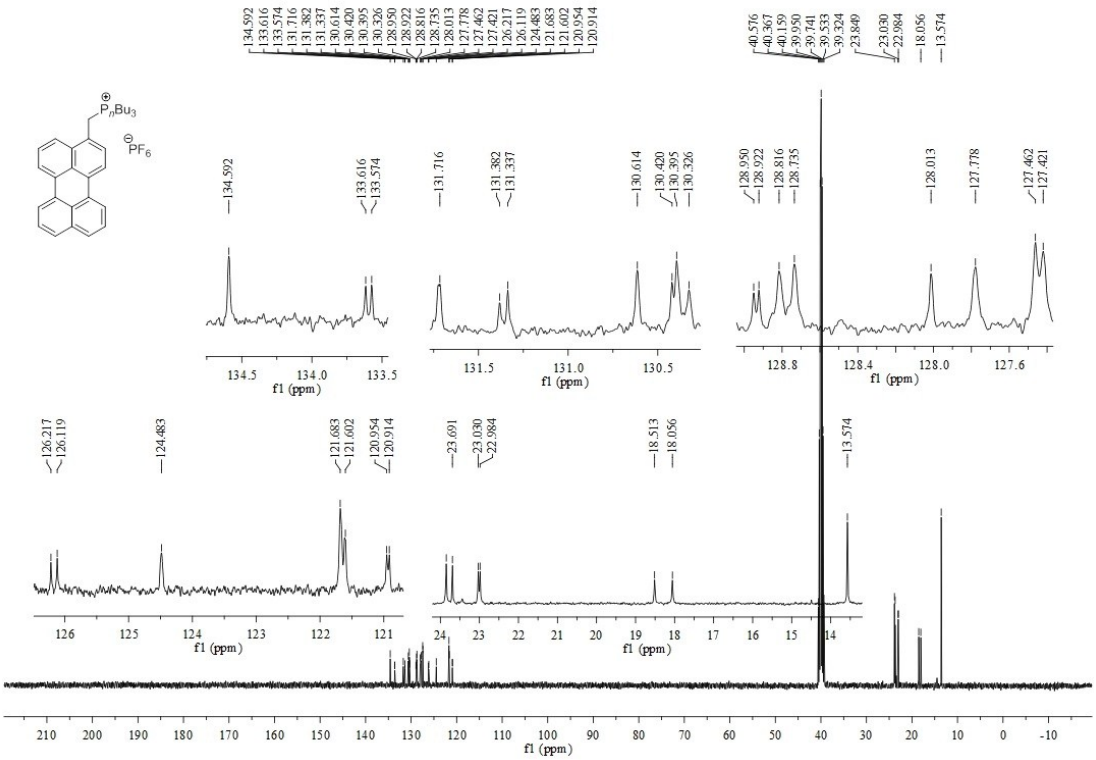
P$_n$Bu$_3$
PF$_6$
f1 (ppm)

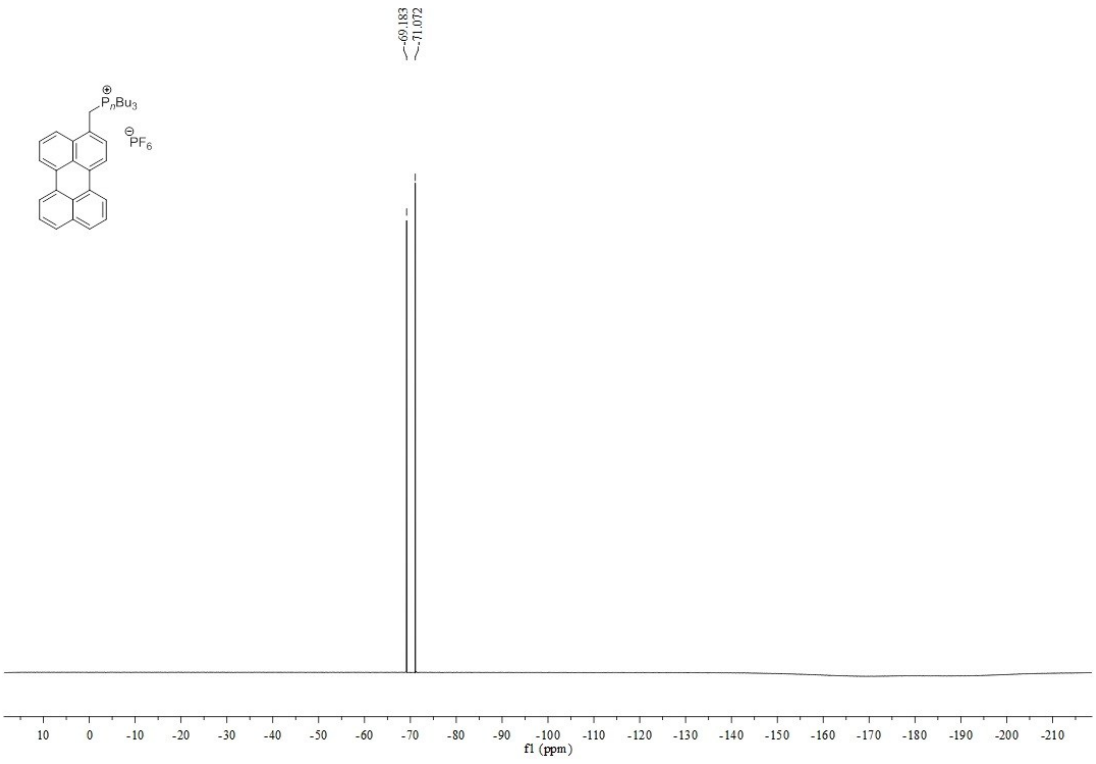
P$_n$Bu$_3$
PF$_6$
f1 (ppm)

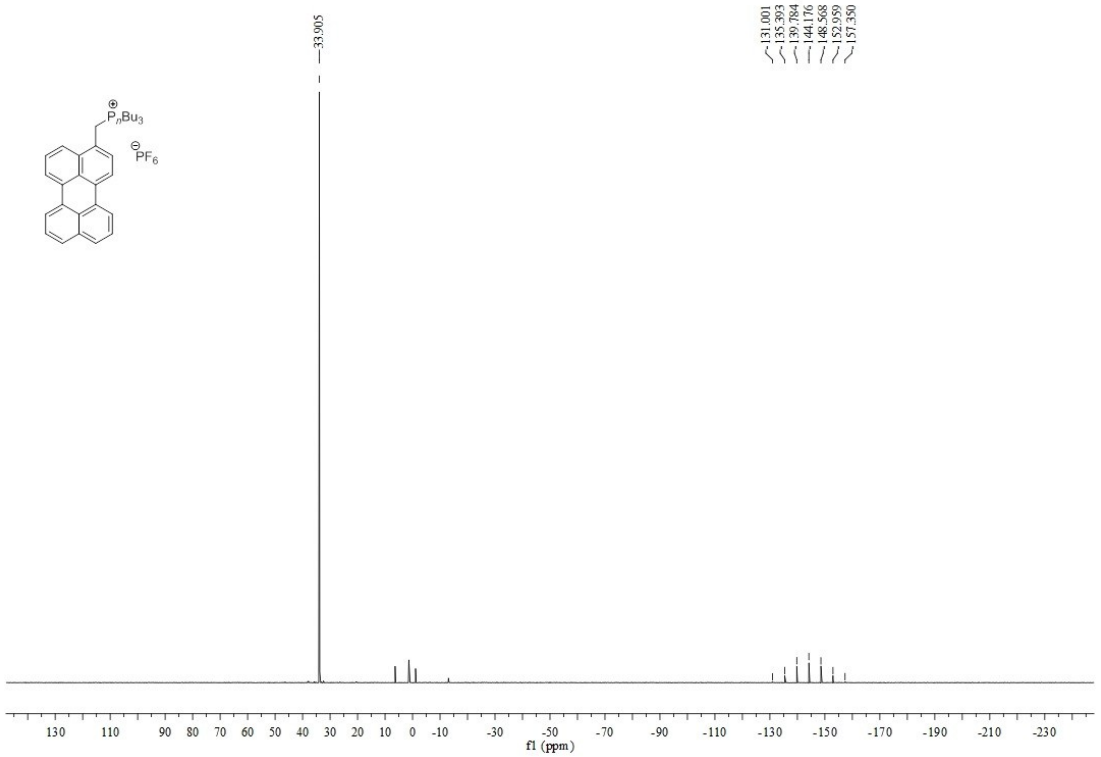
33.905
131.001
135.393
139.784
144.176
148.568
152.959
157.350
f1 (ppm)

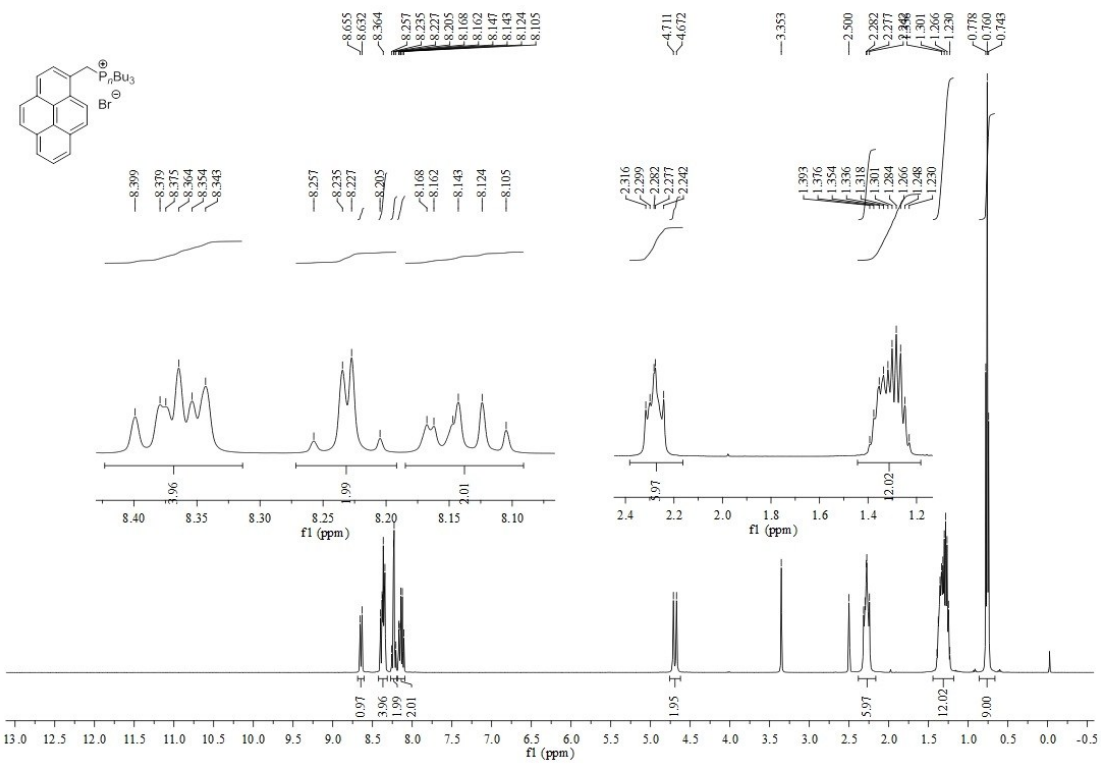
8.655
8.632
8.364
8.257
8.235
8.227
8.205
8.168
8.162
8.147
8.143
8.124
8.105
4.711
4.672
3.353
2.500
2.316
2.299
2.282
2.277
2.242
1.393
1.376
1.354
1.336
1.318
1.301
1.284
1.266
1.248
1.230
0.178
0.160
0.143
3.96
1.99
2.01
5.97
12.02
f1 (ppm)

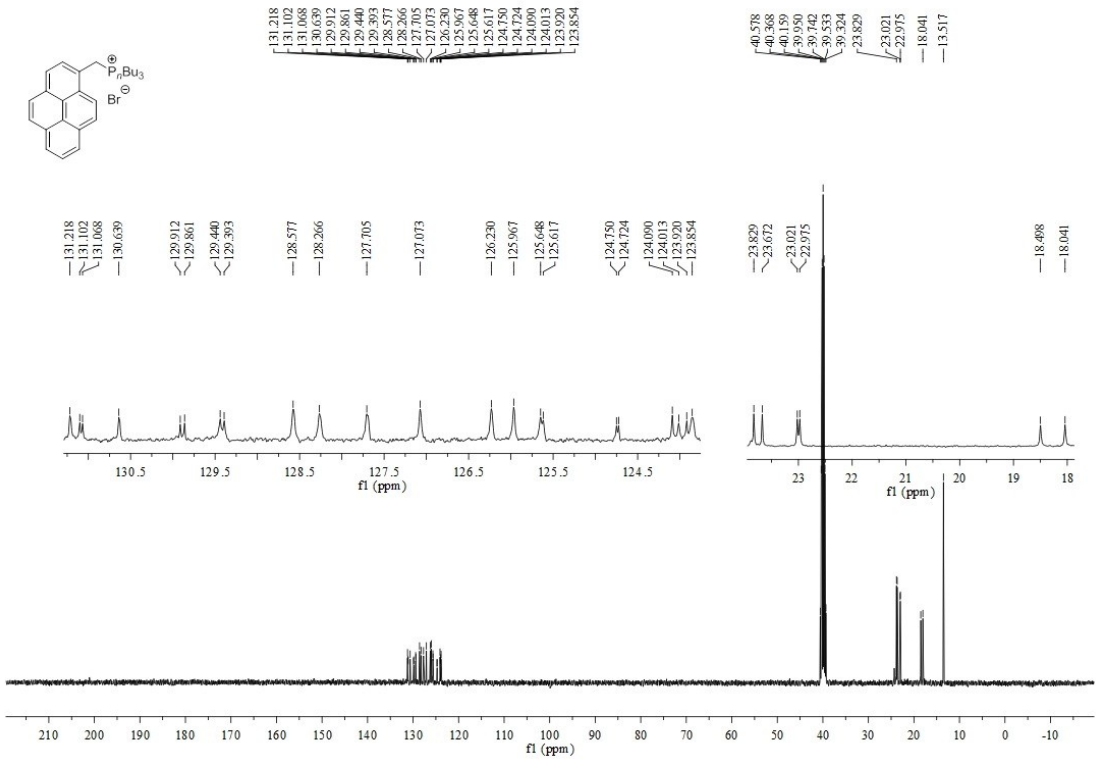
131.218
131.102
131.068
130.639
129.912
129.861
129.440
129.393
128.577
128.266
127.705
127.073
126.230
125.967
125.648
125.617
124.750
124.724
124.090
124.013
123.920
123.854
40.578
40.368
40.159
39.950
39.742
39.533
39.324
23.829
23.021
22.975
18.041
13.517
f1 (ppm)

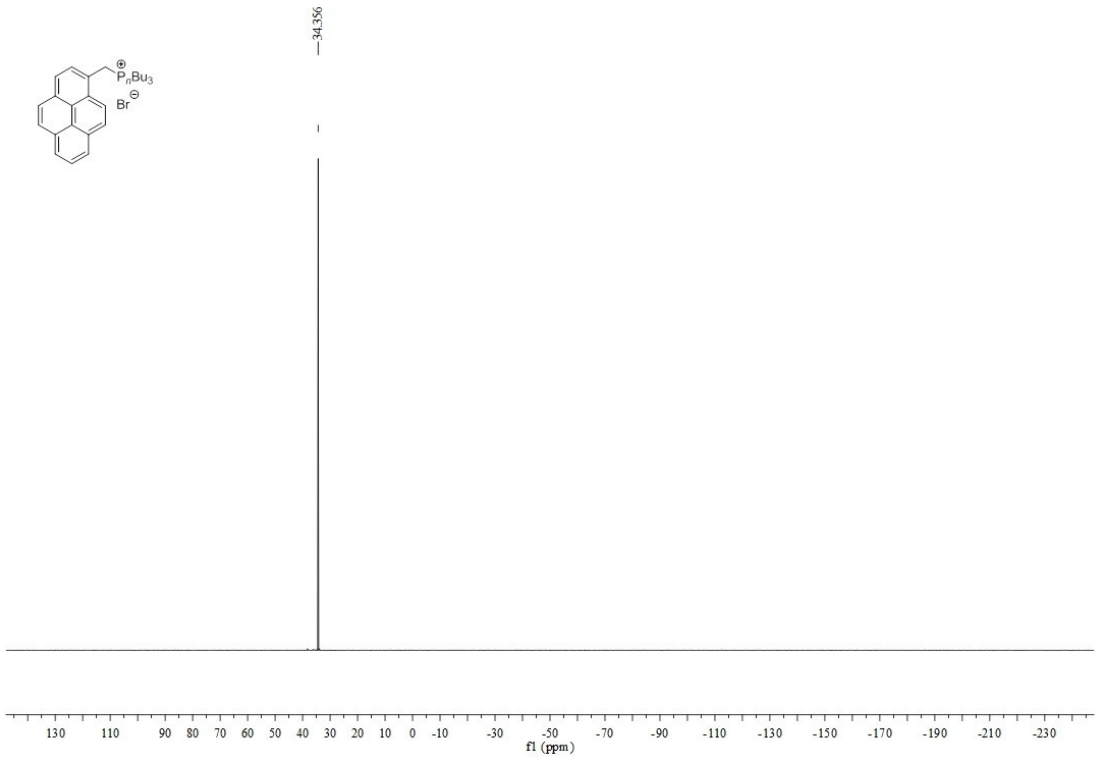
34.356
f1 (ppm)